Rossby Wave Phase Speeds and Mixing Barriers in the Stratosphere. Part I: Observations

KENNETH P. BOWMAN

Climate System Research Program and Department of Meteorology, Texas A&M University, College Station, Texas

(Manuscript received 21 April 1995, in final form 4 October 1995)

ABSTRACT

Lagrangian trajectories are used to calculate isentropic mixing properties for unfiltered and filtered Southern Hemisphere stratospheric winds. In wintertime significant mixing is confined to the surf zone between the Tropics and the edge of the polar vortex. The mixing barrier at the edge of the vortex is located near the core of the polar jet stream (where the maximum wind speeds occur), which is also approximately where the meridional potential vorticity gradient is largest. In summer there is significant mixing throughout the hemisphere, and no high-latitude mixing barrier exists.

When the winds are filtered by zonal wavenumber to retain either the planetary-scale waves (1–3) or the smaller-scale waves (4–12), mixing in the surf zone is generally reduced but not eliminated. When the winds are filtered by phase speed, however, mixing is significantly reduced in restricted latitude zones where the phase speeds of the filtered waves are close to the speed of the local zonal-mean zonal wind. These results indicate that mixing primarily occurs near the critical lines for Rossby waves, where the waves would be expected to break. The presence of the mixing barrier around the polar vortex can be interpreted as a result of the lack of waves with fast phase speeds comparable to the speed of the jet. Artificially amplifying the fast-moving waves can destroy the mixing barrier around the vortex. In summer, when winds are weaker, waves break throughout the hemisphere and the mixing barrier disappears.

1. Introduction

Observational, theoretical, and numerical modeling studies have shown that the wintertime polar vortices in the lower and middle stratosphere contain strong barriers to mixing that effectively isolate the interiors of the vortices from the exteriors (Juckes and McIntyre 1987; McIntyre 1989; Hartmann et al. 1989; Schoeberl et al. 1989, 1992; Bowman 1993a,b; Pierce and Fairlie 1993; Waugh et al. 1994; Dahlberg and Bowman 1994, 1995; Chen et al. 1994; Chen 1994; Pierce et al. 1994a,b). This isolation is especially strong in the Southern Hemisphere, where the wintertime vortex persists into the spring season and the Antarctic ozone hole forms in the cold, sunlit conditions of the vortex interior. Isentropic trajectory calculations by Bowman (1993b), Chen et al. (1994), Chen (1994), and Pierce et al. (1994a,b) show that the interior of the vortex is surrounded by a nearly impenetrable barrier, reducing mixing and exchange of air between the interior and exterior of the vortex to nearly zero, at least until the vortex breaks down in middle to late spring. The Arctic vortex is more perturbed than the Antarctic, and as a result it breaks down earlier, before a large, distinct ozone hole can form. Despite the deformation of the Arctic vortex by the large-amplitude waves of the Northern Hemisphere, it remains relatively well isolated from midlatitude air (Dahlberg and Bowman 1994). Both vortices are eroded from the edge by breaking planetary-scale waves that produce long narrow filaments of air by folding and stretching of material lines (McIntyre and Palmer 1983; Leovy et al. 1985; Bowman and Mangus 1993; Waugh et al. 1994). Large-amplitude distortions of the Arctic polar vortex can also allow some intrusion of midlatitude air into the vortex (Plumb et al. 1994; Dahlberg and Bowman 1994). Nakamura and Plumb (1994) have shown that whether the wavebreaking events break into or out of the vortex depends on the detailed shape of the wind profile and that the observed wind profiles favor outward wavebreaking. The direction of wavebreaking would determine whether entrainment into the vortex or ejection outward would be the dominant mixing mechanism during periods when mixing does occur, which is typically late winter or early spring.

Aside from the direction of wavebreaking, an important question that remains is *why* the vortices have such strong barriers to mixing. McIntyre (1989) proposed that the strong potential vorticity (PV) gradients of the jet are resistant to meridional displacements through the Rossby wave restoring mechanism. Another important factor is the location of critical lines for the large-scale waves in the stratosphere. Randel and Held (1991) showed that Rossby waves tend to break (as indicated by Eliassen–Palm flux diver-

Corresponding author address: Dr. Kenneth P. Bowman, Climate System Research Program, Department of Meteorology, Texas A & M University, College Station, TX 77843-3150.

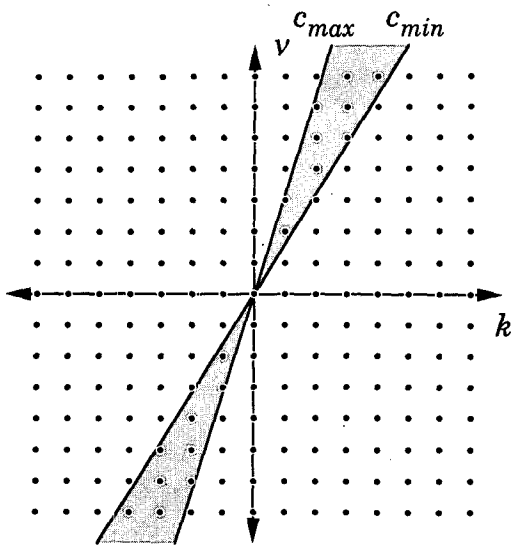

FIG. 1. Schematic showing the locations of discrete components of the space–time spectrum in the zonal wavenumber-frequency ($k-\nu$) plane and an example of a "band-gap" phase speed filter (shaded area).

gences) in latitude zones close to their critical lines. When the phase speed of a wave matches the speed of the basic-state flow, an air parcel remains stationary with respect to the phase of the wave. Rather than moving through the wave and experiencing an oscillating meridional velocity (and oscillating meridional displacements), the parcels have a nearly constant meridional velocity and can "surf" in the meridional direction. This process is usually limited by the shear in the background flow. As the parcel moves into a region where its zonal velocity no longer matches the phase speed of the wave it loses the wave. The result is the classic Kelvin's cat's eye of a breaking wave.

Monochromatic waves tend to mix vigorously in a zone near their critical lines. The width of the mixing zone for a single wave depends on the amplitude of the wave and the background shear (Bowman 1995). Using a global equivalent barotropic model, Salby (1992) showed that transience in the planetary waves tends to spread the spectrum in frequency or, equivalently, in phase speed. As a result, mixing occurs through a wider latitudinal zone but at a slower rate. Bowman (1993b) showed that in a shallow-water-type model the dominant observed waves in the Southern Hemisphere (stationary zonal wavenumber 1 and eastward-moving zonal wavenumber 2) mix strongly in the subtropics and on the equatorial flank of the polar vortex (by wavebreaking) but do not mix midlatitude and vortex air across a barrier that is roughly coincident with the jet maximum. The eastward phase speed of the wavenumber 2 disturbance is substantially less than the maximum wind speed during the winter and most of the spring. In late spring the jet slows to near the phase speed of the wave 2 disturbance, the entire interior of the vortex becomes a "critical zone," and the vortex breaks down rapidly. This suggests as a hypothesis that the mixing barrier around the polar vortices results from the absence of waves with eastward phase speeds as fast as the wind speeds at the jet maxima. With no critical lines near the core of the jet, there is no wavebreaking and little mixing. The jet maxima are also regions of strong PV gradients, so the absence of critical lines and a strong resistance to meridional displacement together produce the mixing barrier. The polar vortex is resistant to mixing even when unstable (Bowman and Chen 1994).

Bowman (1995) proposed a simple model of diffusive mixing resulting from repeated breaking of waves with varying critical line locations (varying phase speeds with respect to the mean flow). In that simple kinematic model, a mixing barrier is created by a latitude zone in which no critical lines occur.

The absence of critical lines near the jet maxima does not imply the absence of planetary-scale waves. In fact, wave amplitudes are largest near the jet core (Randel 1992). Since the flow is moving faster than the waves and there are no critical lines in that region, however, even large amplitude waves produce reversible displacements. Parcels are carried through the wave so quickly by the high-speed zonal flow that they are reversibly displaced poleward and equatorward, rather than "surfing" and breaking with the wave. Waves propagate nearly vertically through this region from the upper troposphere, first decelerating the basic state and then reaccelerating it as they propagate into the middle and upper stratosphere. In the lower stratosphere the net deceleration from the waves is weak. The strongest dissipation tends to occur higher and on the equatorward flank of the jet in the surf zone (Randel 1990).

In a companion paper, the relationship between the phase speed of the waves and the mixing barrier is tested further using a global equivalent-barotropic model by forcing waves with known phase speeds on a specified basic state. Here we use observed winds to test the hypothesis that the mixing barrier is a result of the absence of waves with phase speeds close to the speed of the jet maxima. Reasons for the absence of fast eastward-moving waves are discussed in the conclusions.

2. Data and methods

a. Data

The principal technique used here to analyze large-scale horizontal mixing is area-filling trajectory calculations. Large numbers of passive Lagrangian tracer parcels are initialized throughout a wide latitude band on an isentropic surface in the lower stratosphere. The isentropic trajectories of the parcels are computed numerically using the analyzed winds. The data source

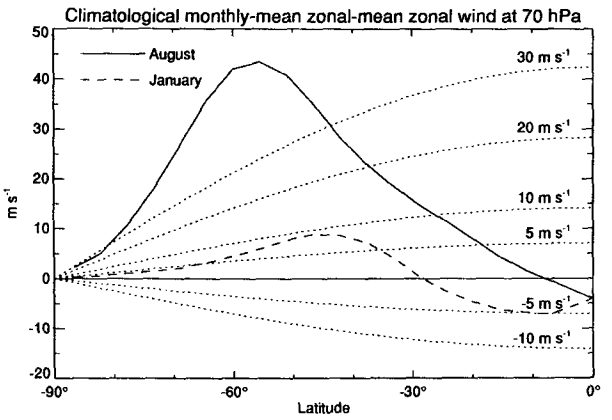

FIG. 2. Climatological monthly mean zonal-mean zonal wind at 70 hPa for August and January and local phase speeds for waves with constant angular velocities. The labels indicate the phase speed of the waves at 45°.

for winds is 14 years (1980–1993) of daily (1200 UTC), global, geopotential heights from the Climate Analysis Center stratospheric analysis (70–0.4 mb) and the National Meteorological Center (NMC, currently known as the National Centers for Environmental Prediction) tropospheric–lower-stratospheric analysis (1000–100 mb) that have been assembled into a single data set by Randel (1992). Randel transformed the gridded NMC analyses to zonal Fourier components (up to wavenumber 12) on a 40-point Gaussian grid. Some gaps were interpolated in time, and some bad values have been replaced by interpolated values. Details of the dataset and known problems can be found in Randel (1992) and Trenberth and Olson (1987).

b. *Methods*

Temperatures are computed from the hydrostatic equation using finite differences in log pressure. Winds are derived from geopotential heights as in Randel (1992). Zonal-mean winds are obtained from the gradient-wind equation. Higher zonal harmonics are obtained from the linear balanced wind equations. The linear wind equations can become singular, in which case geostrophic winds are used.

Lagrangian trajectories are computed for one-month periods on isentropic surfaces using a standard fourth-order Runge–Kutta scheme. Details can be found in Bowman (1993b). The validity of the adiabatic assumption and the accuracy of the trajectory calculations has been discussed in Schoeberl et al. (1992), Bowman (1993b), and Dahlberg and Bowman (1994). Trajectories are calculated for large numbers of parcels (typically $128^2 = 16\,384$) initially arranged on a regular longitude–latitude grid. Halving or doubling the number of parcels produces only small changes in mixing statistics, so the mixing statistics do not appear to be sensitive to the number of parcels at this resolution.

The geopotential height fields are filtered in various ways before winds are computed. The control case uses unfiltered winds. The simplest filters remove different spatial scales by zonal wavenumber. Two different spatial filters are used: the first in which waves 4–12 (medium-scale and smaller waves) are removed, and the second in which waves 1–3 (planetary-scale waves) are removed.

The second type of filter removes waves by zonal phase speed. The filtering is carried out in the spectral domain. The geopotential heights at each latitude and pressure are expanded in a space–time Fourier series as

$$Z(\lambda_i, t_s) = \sum_k \sum_\nu z_{k,\nu} e^{i(k\lambda - \nu t)}, \qquad (1)$$

where Z is the geopotential height, the λ_i are the longitude grid points, the t_s are the daily time samples, k and ν are discrete spatial and temporal frequencies (k is the zonal wavenumber), and $z_{k,\nu}$ is the complex amplitude of each wave. The complex two-dimensional spectrum, $z_{k,\nu}$, is computed using fast Fourier transforms; the spectrum is multiplied by a filter that depends on the phase speed of each traveling wave component, $c = \nu/k$; and the inverse transform is computed to produce the filtered height fields. Three different sample lengths were tested for the temporal transform: 32-, 64-, and 128-day periods centered on the month of interest. Changing the length of the sample had minimal effect on the mixing statistics; results shown here are for a 64-day window.

Since observed wave modes tend to be coherent in that they propagate with angular velocities that are independent of latitude, the phase speed c (in degrees of longitude per day) is computed for each wavenumber–frequency pair in the transformed field; and the amplitudes of components with phase speeds falling in the range $c_{\min} \leqslant c \leqslant c_{\max}$ are set to zero. If $c_{\min} > -\infty$ and $c_{\max} = \infty$ the filter is a low-pass filter, while if $c_{\min} = -\infty$ and $c_{\max} < \infty$ it is a high-pass filter. If $c_{\min}$ and $c_{\max}$ are both finite, the filter is a "band-gap" (rather than a bandpass) filter. The band-gap filter is illustrated in Fig. 1. Dots indicate the discrete spatial and temporal frequencies for $\pm k$ and $\pm\nu$. (Since the input data are real, the spectral components reflected through the origin are complex conjugates.) For the band-gap filter, spectral components falling within the shaded area are set to

TABLE 1. Period of a wavenumber 1 disturbance for selected phase speeds at 45° latitude.

Phase speed (m s^{-1})	Period (days)
5	65.6
10	32.8
20	16.4
30	10.9
40	8.2

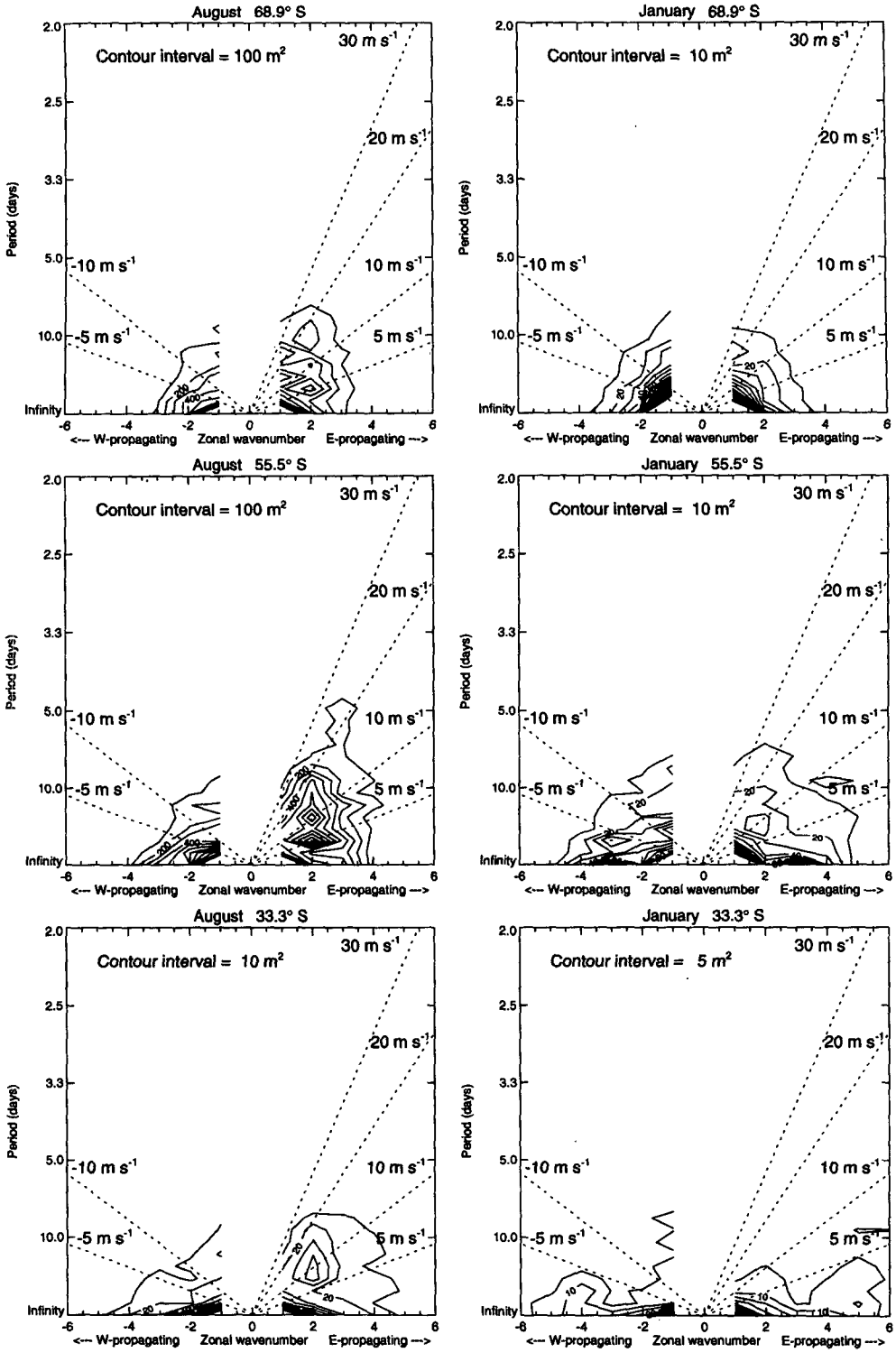

FIG. 3. Ensemble-mean space–time power spectra at 70 hPa for August and January at three different latitudes: 68.9°S (inside the wintertime polar vortex), 55.5°S (in the midlatitude surf zone), and 33.3°S (in the subtropics). Some contour lines near the large peaks for stationary wave 1 are omitted for clarity. The dotted lines are isopleths of phase speed as a function of wavenumber and frequency. The labels give the phase speed relative to the ground at 45°S. The contour interval for each plot is indicated.

zero. The zonal-mean components ($k = 0$) are always left unchanged by the filter. The stationary wave components ($\nu = 0$) may be affected, depending on the choice of filter limits. Note that the phase speed of a coherent wave relative to the ground (in m s^{-1}) depends on latitude. The filter used here removes waves with the same *angular velocity* at each latitude, rather than waves with the same phase speed relative to the ground. In the tables and figures the phase speed filters are labeled by the phase speed of the waves relative to the ground at 45°S to make it easier to compare wave phase speeds with the speed of the zonal wind.

In a few cases the space–time spectra have been "antifiltered." That is, the spectral components within a phase-speed band have been multiplied by a factor greater than 1.0 to increase their amplitudes. This makes it possible to evaluate the effect of a hypothetical increase in the amplitude of waves with certain phase speeds. In all cases, effective diffusion coefficients are estimated from the trajectories for each month from the rate of increase of the variance of parcel latitudes (Schoeberl et al. 1992; Bowman 1993).

3. Results

a. Basic-state wind profiles and wave spectra

Trajectories are computed with unfiltered winds on the 500 K isentropic surface for every month of the 14-yr dataset. Statistics are ensemble-averaged by calendar month. For brevity, results from two months are presented here: August (winter) and January (summer). Some aspects of the seasonal cycle of mixing can be seen in Bowman (1995). Climatological monthly mean zonal-mean zonal winds are plotted in Fig. 2 for the two months. The maximum wind speed in August is greater than 40 m s^{-1}, while the maximum in January is less than 10 m s^{-1}. The average latitude of the center of the jet is about 55°S in August, but the jet moves equatorward in January, so that the jet maximum lies near 45°S at this level. The zero-wind line also moves from approximately 10°S in August to 30°S in January. The dotted lines in Fig. 2 show the local phase speed relative to the ground (in m s^{-1}) for wave modes with constant zonal angular velocities. The labels indicate the phase speed at 45° latitude. The periods for a wavenumber 1 disturbance with the given phase speeds are listed in Table 1 for reference.

Traveling wave power spectra for the two months are shown in Fig. 3 for the 70-mb geopotential heights at three latitudes: 33.3°, 55.5°, and 68.9°S. These power spectral estimates were computed by ensemble averaging the 14 raw periodograms for the individual years. Note that the contour intervals vary between the different graphs. The stationary wave components lie along the abscissa (infinite period). The zonal-mean components (wavenumber 0) have been omitted. The dotted lines indicate the zonal phase speeds for the waves. The largest component by far in all of the plots is the stationary wave 1. In some of the graphs, some contour lines are omitted near the stationary wave 1 peaks for readability. In general, the bulk of the variance is at periods longer than 10 days and wavenumbers lower than 4. During the summer (January), there is relatively more power at higher wavenumbers. Near the jet in winter (August, 55.5°S) there is some power between 5 and 10 days.

The fractional variance within the various phase speed bands is given in Table 2. In August waves near the jet core with phase speeds faster than 20 m s^{-1} typically amount to about 10% of the total wave variance. Eastward-moving waves, excluding stationary waves, comprise about 50% of the total variance; the stationary waves are about 20%–30% of the variance; and the westward-propagating waves, therefore, are the remaining 20%–30% of the total variance. During January the eastward moving waves amount to relatively less of the total variance, while the stationary and eastward-moving waves comprise a larger fraction.

b. Unfiltered trajectories

The dispersion of the parcels in the surf zone and inside the vortex is illustrated in Figs. 4a and 4b by plotting the locations of two subsets of parcels at the beginning and end of the 1-month trajectory calculations. Results from all 14 years of the 1-month integrations are plotted in each figure. The upper left panel of

TABLE 2. Percentage wave variance in selected phase-speed bands.

Phase speed range (m s^{-1})	Latitude		
	−68.9°	−55.5°	−33.3°
		August	
$30 < c < \infty$	6.5	3.1	2.4
$20 < c < \infty$	14.5	10.5	7.4
$10 < c < \infty$	29.7	30.3	25.2
$0 < c < \infty$	45.9	50.6	48.8
$0 \leq c < \infty$	76.2	77.9	71.5
$c = 0$	30.3	27.3	22.8
$-\infty < c \leq 0$	54.1	49.4	51.2
$-\infty < c < 0$	23.8	22.1	28.5
$-5 < c < 5$	37.7	37.1	37.6
$-10 < c < 10$	56.2	59.2	59.8
		January	
$30 < c < \infty$	3.8	4.0	3.9
$20 < c < \infty$	6.7	8.4	7.1
$10 < c < \infty$	14.5	18.8	17.8
$0 < c < \infty$	25.5	35.3	45.6
$0 \leq c < \infty$	67.8	72.8	61.0
$c = 0$	42.3	37.5	15.5
$-\infty < c \leq 0$	74.5	64.7	54.4
$-\infty < c < 0$	32.2	27.2	39.0
$-5 < c < 5$	47.5	49.3	40.0
$-10 < c < 10$	67.1	66.5	61.5

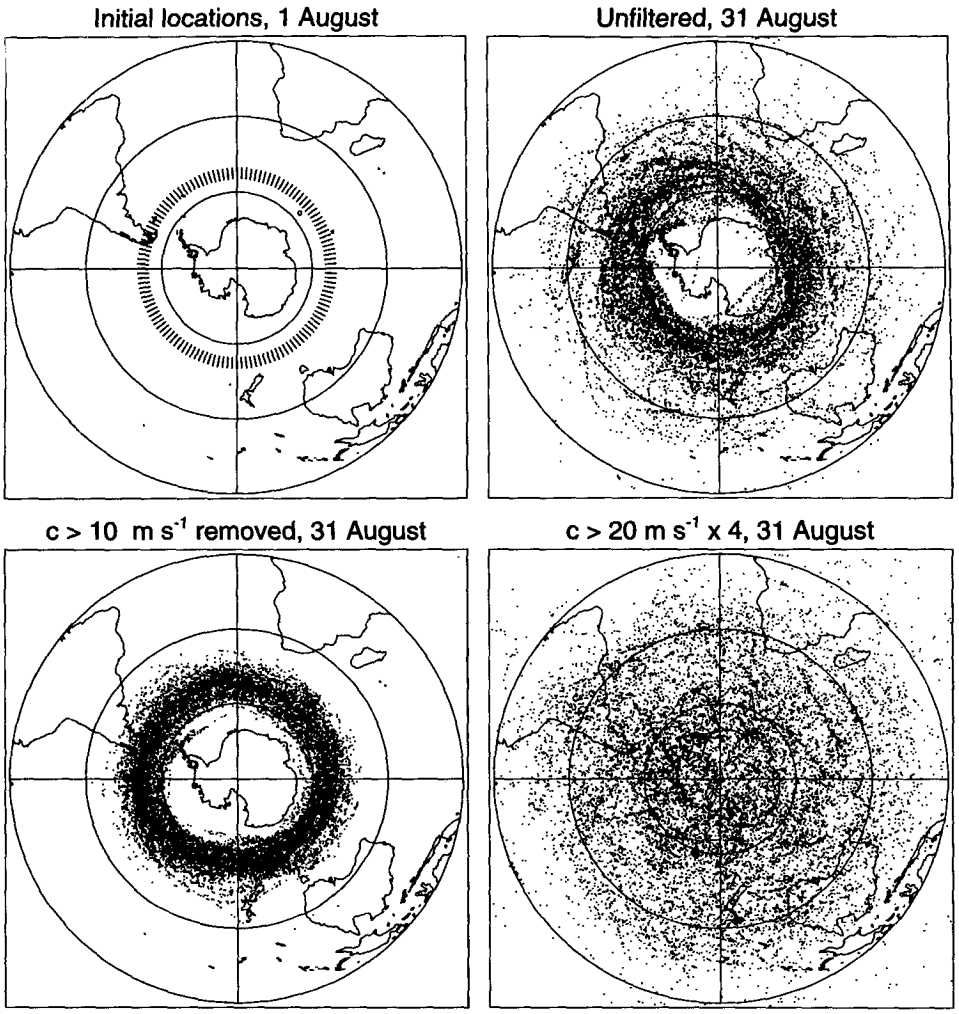

FIG. 4. (a) Ensemble parcel dispersion (1980 through 1993) for several filtered and unfiltered trajectory calculations for the month of August. Top left: initial parcel locations on 1 August (50°–55°S). Top right: parcel locations on 31 August using unfiltered winds. Bottom left: parcel locations on 31 August using winds with waves with phase speeds $c > 10$ m s^{-1} removed. Bottom right: parcel locations on 31 August using winds with waves with $c > 20$ m s^{-1} amplified by a factor of 4.

Fig. 4a shows the locations at the start of the integration (1 August). In this case the subset consists of all parcels initially between 50° and 55°S. These parcels are in the surf zone just outside of the polar vortex. The upper-right panel shows the locations of those parcels at the end of August, with trajectories computed using unfiltered wind fields. During the course of the month the parcels disperse through the midlatitudes but do not penetrate into the polar vortex. Because the figure superimposes the results from 14 individual months, the boundary of the polar vortex appears fuzzy. In fact, the vortex boundary for each individual year is quite distinct, and the fuzziness is due to the superposition of the varying vortex boundary locations on 31 August of the available years. The top two panels of Fig. 4b show similar results for parcels originally located inside the vortex between 70° and 75°S. In this case the parcels do not escape from the vortex into the surf zone but remain closely confined. The bottom panels in Figs. 4a and 4b are discussed below.

Figure 5 shows a similar set of maps for January. In this case the subset consists of those parcels initially located between 20° and 25°S. This latitude zone is on the equatorward side of the jet maximum. Parcels are dispersed throughout the hemisphere, and it is clear that there is no mixing barrier around the weak polar vortex in summer (top right panel). Parcels initially located at high latitudes also mix throughout the hemisphere (not shown).

The mixing behavior for the two months is summarized by estimated diffusion coefficients plotted as a function of latitude in Fig. 6 (solid lines). The iso-

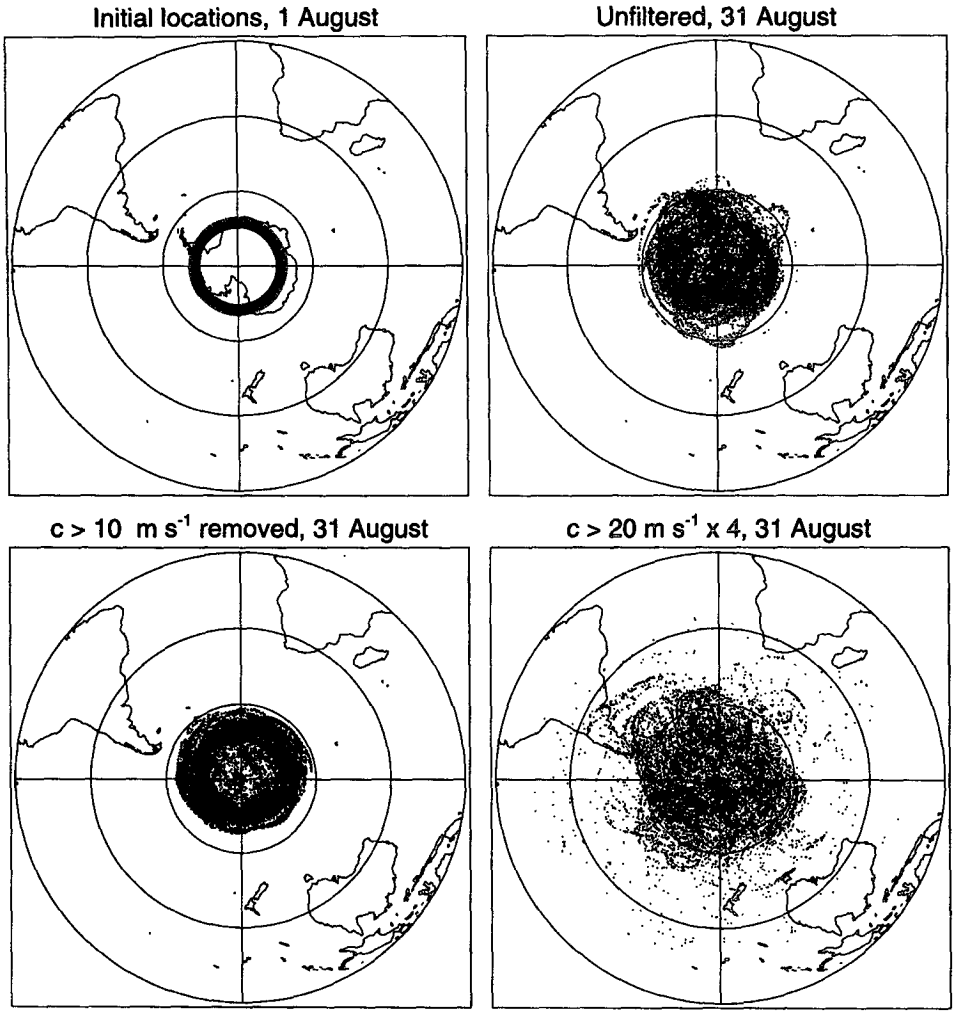

FIG. 4. (*Continued*) (b) As in (a) except that the initial parcel locations are inside the vortex (70°–75°S).

lation of the wintertime vortex is clearly evident, with the vortex boundary or mixing barrier lying slightly equatorward of 60°S. At that latitude the mixing rate jumps dramatically and then increases through the mid-latitude surf zone into the Tropics. Note that the mixing barrier coincides closely with the maximum wind speed in the jet (Fig. 2). In January the maximum mixing rates are somewhat lower, and there is no longer any evidence of a mixing barrier around the polar vortex, as the diffusion coefficients remain high throughout the hemisphere.

c. *Filtering by zonal wavenumber*

Figure 6 also shows the diffusion coefficients for wind fields that have been filtered by zonal wavenumber k. Two filters are used: a low-pass filter (waves 4 through 12 removed) and a high-pass filter (waves 1 through 3 removed). The diffusion coefficients indicate that in August the large-scale waves are more important than the smaller-scale waves just outside the vortex, but elsewhere the two wavenumber bands are roughly equally important. In January the large-scale waves are more important near the pole (this is probably an effect of the spherical geometry), while the smaller-scale waves are more important in the Tropics and subtropics. In neither case is it possible, however, to attribute the bulk of the mixing to waves with particular spatial scales.

d. *Filtering by phase speed*

Results from the calculations with low-pass and high-pass phase speed filters are shown in Figs. 7 and 8, respectively. As in Fig. 6 the diffusion coefficients from the unfiltered runs are plotted for comparison (solid lines). In Fig. 7 the other curves indicate the diffusion coefficients for low-pass filtered winds as the

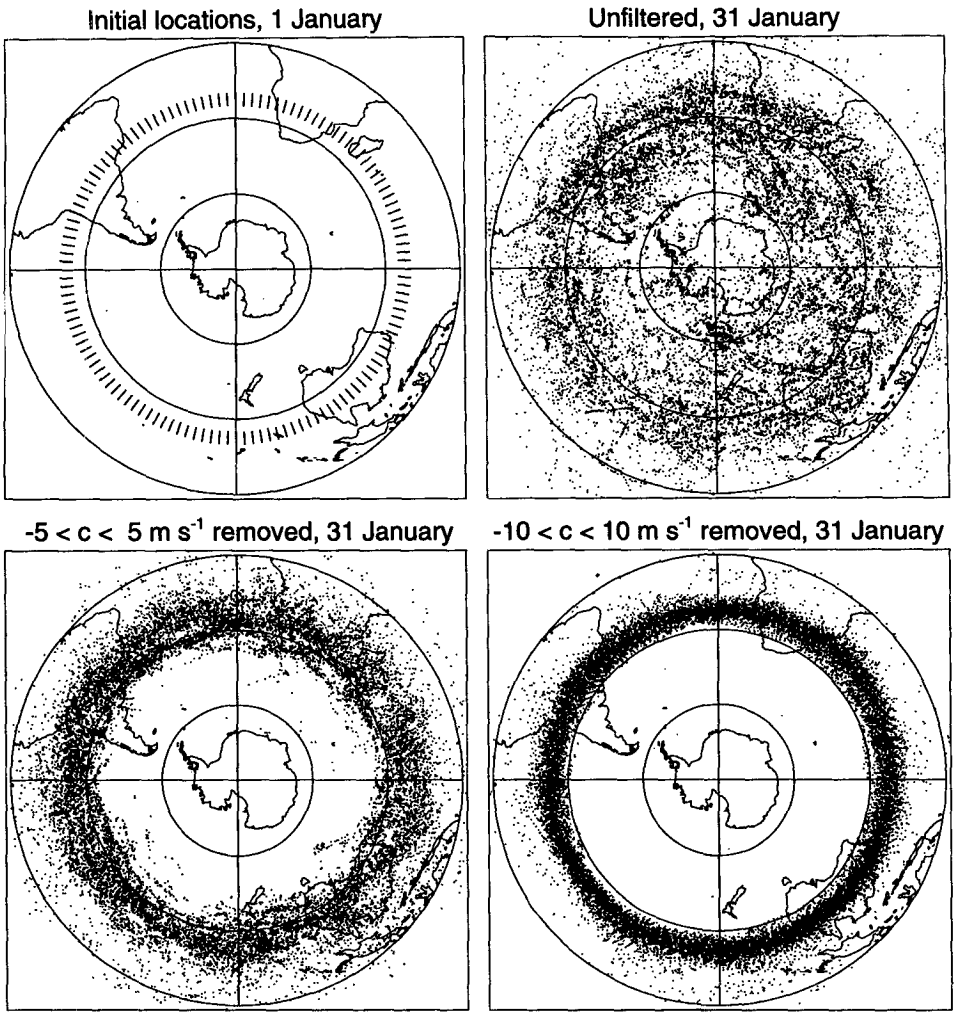

FIG. 5. Ensemble parcel dispersion (1980 through 1993) for several filtered and unfiltered trajectory calculations for the month of January. Top left: initial parcel locations on 1 January (20°–25°S). Top right: parcel locations on 31 January using unfiltered winds. Bottom left: parcel locations on 31 January using winds with waves with $-5 < c < 5$ m s^{-1} removed. Bottom right: parcel locations on 31 January using winds with waves with $-10 < c < 10$ m s^{-1} removed.

upper limit of the filter is reduced and progressively slower eastward-propagating waves are removed from the wind fields. The labels indicate the upper cutoff of the low-pass filter. Thus, $c > 20$ m s^{-1} indicates that all waves with phase speeds greater than 20 m s^{-1} (at 45°S) are removed. In Fig. 7 it is clear that mixing is steadily reduced beginning at the vortex edge as slower and slower waves are removed. Thus, as expected, the fastest waves mix primarily where the winds speeds are highest, on the flank of the jet. Mixing in the subtropics decreases significantly only when the stationary waves are removed, as would be expected with a zero-wind line located in the nearby Tropics.

The end of month parcel locations for one of the low-pass-filtered cases ($c > 10$ m s^{-1} removed) is shown in the lower left panels of Figs. 4a and 4b. As expected, removing the fast waves greatly reduces the parcel dispersion on the flank of the jet (Fig. 4a). Parcels initially inside the vortex (Fig. 4b) are confined as before.

Comparing the low-pass results for August in Fig. 7 with the high-pass results in Fig. 8 emphasizes the importance of the eastward-propagating waves. Removing all westward-propagating waves (negative phase speeds) has only a small effect on the mixing, reducing it on the order of 25% in the subtropics and midlatitudes. Mixing on the flank of the jet, where wind speeds are higher, is hardly affected at all. If the stationary waves are removed as well, the mixing decreases to approximately one-half of its unfiltered value in the Tropics, but there is still little change near the vortex boundary, further illustrating the importance of the fast

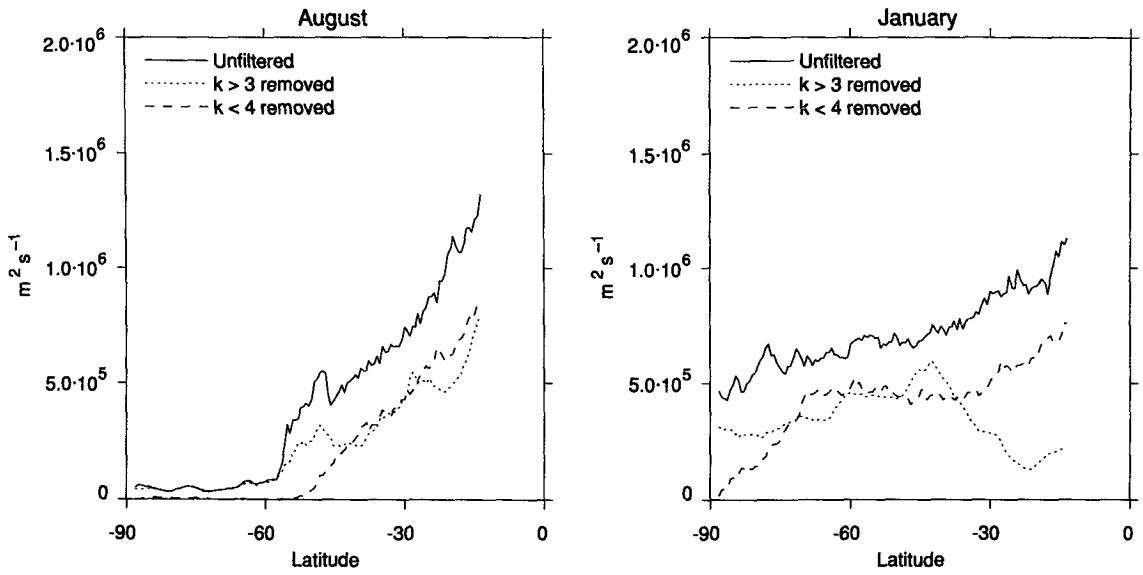

FIG. 6. Diffusion coefficients (K_{yy}) as a function of latitude estimated from parcel dispersion statistics for unfiltered winds and winds filtered by zonal wavenumber m.

eastward moving modes in mixing on the equatorward flank of the jet.

Returning to the January results in Fig. 7 it can be seen that removing fast eastward moving waves ($c > 10$ m s^{-1}) has almost no effect on the flow, which is expected since they comprise only a very small portion of the total wave variance and the maximum wind speed is less than 10 m s^{-1} on average. As the slower-moving and stationary waves are removed, however, the mixing decreases substantially throughout the hemisphere. As in the August case, the westward-propagating waves have much less impact on the mixing (Fig. 8), until the stationary waves are removed.

From earlier results it can be seen that removing fast eastward-moving waves reduces the mixing where winds speeds are high—on the flank of the jet. Conversely, we would expect that removing slow eastward- or westward moving or stationary waves should reduce mixing where winds speeds are low—in the Tropics and subtropics. Figure 9 shows the dif-

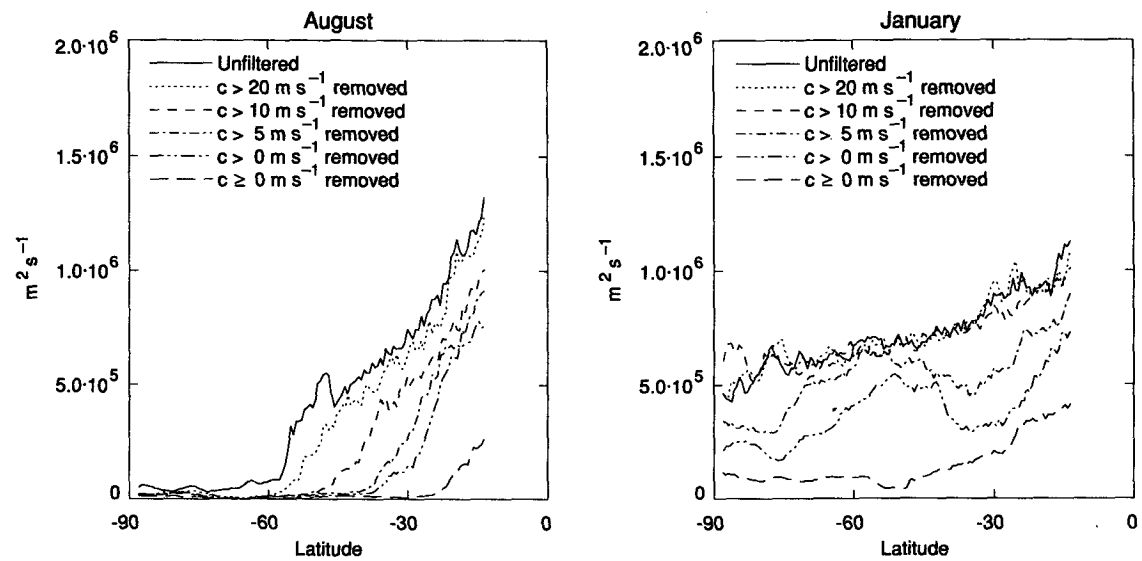

FIG. 7. Diffusion coefficients (K_{yy}) as a function of latitude estimated from parcel dispersion statistics for unfiltered winds and winds low-pass filtered by wave phase speed c. The labels indicate the upper limits of the low-pass filter.

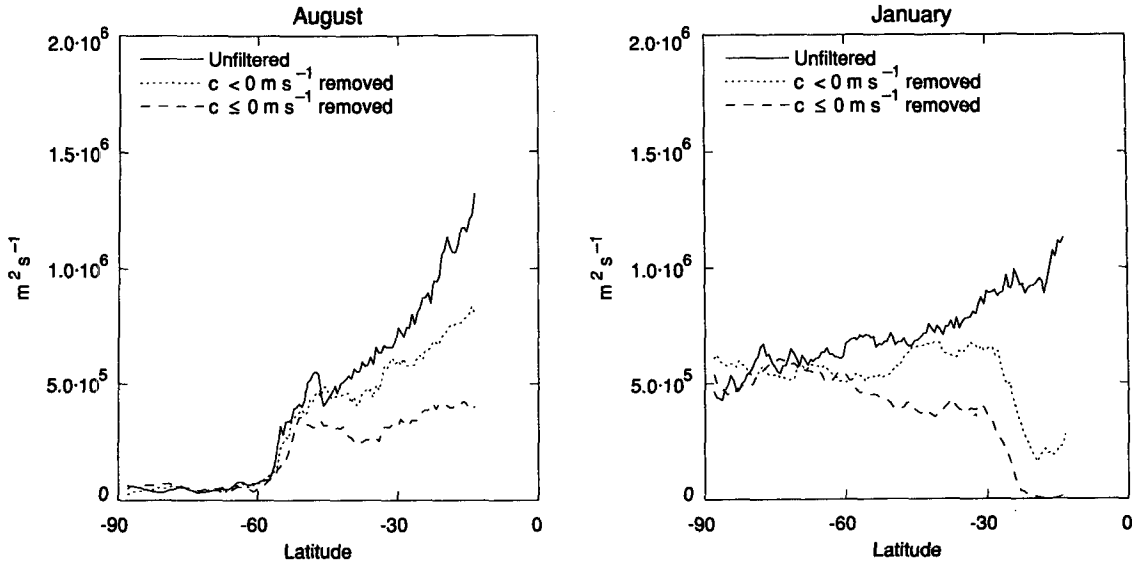

FIG. 8. Diffusion coefficients (K_{yy}) as a function of latitude estimated from parcel dispersion statistics for unfiltered winds and winds high-pass filtered by wave phase speed c. The labels indicate the lower limits of the high-pass filter.

fusion coefficients for the band-gap filtered winds, in which waves with phase speeds between two finite limits are removed. In August, removing only the stationary waves primarily affects the mixing in the subtropics. As the width of the band-gap increases to include slow-moving eastward and westward propagating waves, the reduction in mixing extends into midlatitudes, with the equatorward flank of the jet affected the least. In January, when winds are weaker, mixing is reduced throughout the entire hemisphere.

The effects of eliminating the slow moving waves on the trajectories can be seen in the lower two panels of Fig. 5. When waves with phase speeds between -5 and 5 m s^{-1} are removed, parcels no longer disperse from the subtropics throughout the hemisphere. When a large band-gap is selected (-10 to 10 m s^{-1}), dispersion is reduced even further.

e. Amplifying selected phase speeds

As a final test of the hypothesis that a lack of fast eastward propagating waves is responsible for the mixing barrier around the polar vortex, trajectory calculations are carried out with "antifiltered" winds. In these experiments the amplitudes of the very fastest waves in the observed wind fields are amplified rather than attenuated. Results are shown in Fig. 10 along with the estimated diffusion coefficient for the unfiltered calculations. When the amplitudes of all waves with phase speeds greater than 30 m s^{-1} (eastward moving) are multiplied by a factor of 4, the isolated region of the vortex shrinks poleward, while the mixing increases dramatically in the region of the jet core. In midlatitudes and the subtropics, on the other hand, where wind speeds are lower, the mixing increases much less. As the amplified portion of the phase speed spectrum expands, the isolated part of the vortex continues to shrink and the mixing barrier disappears.

Parcel locations from one case ($c > 20$ m s$^{-1} \times 4$) are shown in the lower right panel of Figs. 4a and 4b. For both vortex and surf zone parcels the mixing barrier disappears. Amplifying only the fastest moving waves ($c > 30$ m s^{-1}) is not sufficient to break the mixing barrier (although it does displace it poleward). Amplifying the slower moving waves, which have critical lines outside the jet, and increasing the width of their critical layers does break the mixing barrier down completely.

4. Conclusions

The trajectory calculations presented here provide strong evidence that Rossby wavebreaking and large-scale mixing in the stratosphere are controlled by the location of wave critical lines (or critical surfaces in a three-dimensional view). The presence of a mixing barrier around the polar vortices in the winter season is due primarily to the absence of waves of significant amplitude with phase speeds as fast as the winds in the core of the jet. The large amplitude waves found near the jet core have phase speeds much lower than the zonal wind, and the relatively large potential vorticity gradients near the jet provide a strong Rossby wave restoring mechanism. As a result, parcel displacements due to the waves are almost entirely reversible. Cooling of the Antarctic stratosphere due to ozone depletion should, therefore, tend to increase the strength of the jet (through thermal wind balance) and increase the isolation of the polar vortex.

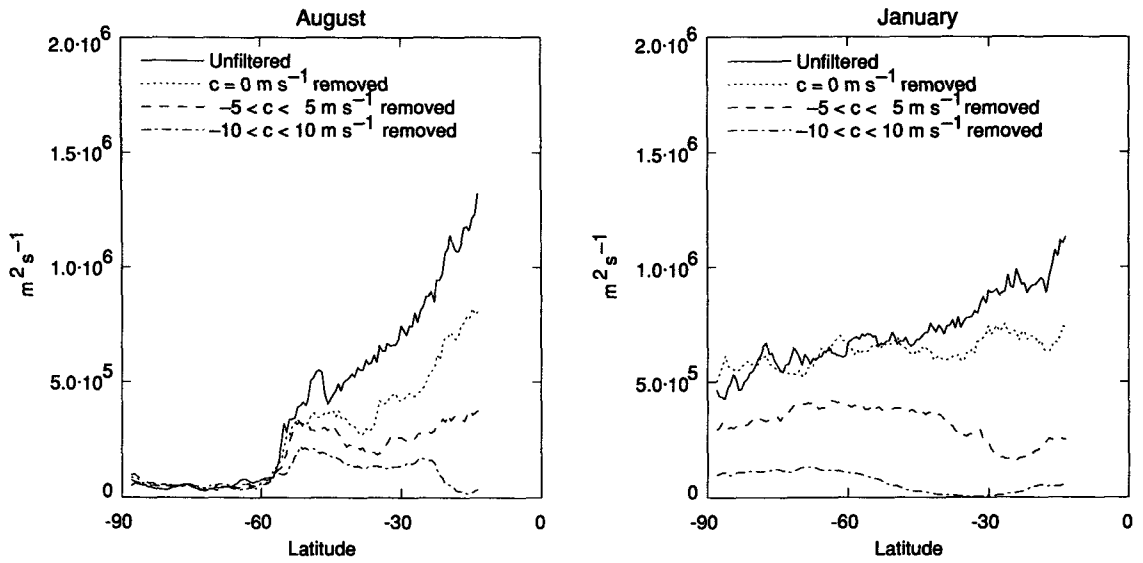

FIG. 9. Diffusion coefficients (K_{yy}) as a function of latitude estimated from parcel dispersion statistics for unfiltered winds and winds band-gap filtered by wave phase speed c. The labels indicate the lower and upper limits of the band-gap filter.

In summer the Southern Hemisphere stratosphere is well mixed on a monthly timescale. Since wind speeds are weak (typically less than 10 m s^{-1}), there are no latitude zones that are free of critical lines and breaking waves. Additional work is currently underway on the transitional seasons and the breakdown of the polar vortex.

These calculations do not provide much information about the subtropical edge of the surf zone since the balance relations used to estimate the winds lose their validity at low latitudes. Therefore, the diffusion coefficients at the subtropical end of the graphs in Figs. 6–10 should be viewed with skepticism. Preliminary results from trajectories calculated from general circulation model winds show good evidence for a mixing barrier on the subtropical side of the surf zone. Those results will be reported separately.

The reasons for the absence of waves with fast phase speeds may be complex. Observed large-scale waves in the stratosphere appear to be primarily waves that originate in the upper troposphere, either from instabilities or nonlinear interactions, from whence they propagate vertically through the stratosphere. If the waves are the result of instabilities, they will have critical lines in the source region in the upper troposphere. An upper limit on the phase speed of the waves would thus be the maximum wind speed in the upper troposphere. Since the stratospheric winds increase with height, stratospheric Rossby waves are propagating into a region of higher wind speeds. Therefore, they will have phase speeds slower than the stratospheric flow and no critical lines near the jet core. If the waves are the result of nonlinear interactions in the upper troposphere, a simple theory for the phase speed of the resultant waves is not available. It is apparent, however, that nonlinear interactions do not produce waves with high phase speeds in this case.

In the upper stratosphere and lower mesosphere some large-scale waves may be the result of local instabilities. [See Randel and Lait (1991) for a summary.] Surprisingly, even when the vortex is barotropically unstable it is still quite resistant to mixing (Bow-

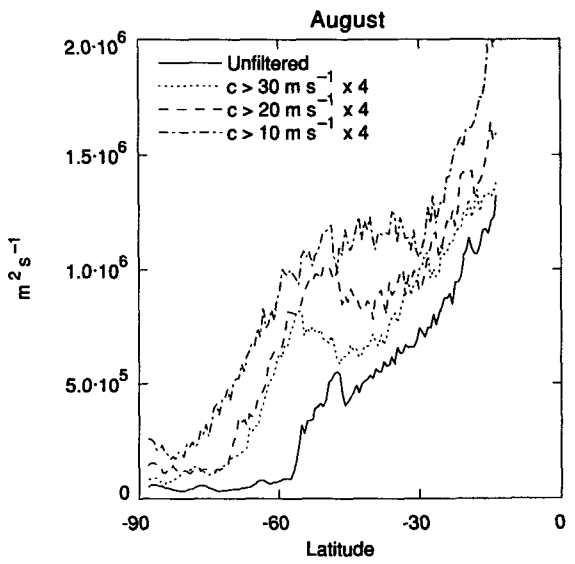

FIG. 10. Diffusion coefficients (K_{yy}) as a function of latitude estimated from parcel dispersion statistics for unfiltered winds and winds antifiltered by wave phase speed c. The labels indicate the lower limits of the amplified part of the phase speed spectrum. Wave amplitudes are increased by a factor of 4.

man and Chen 1994; Ishioka and Yoden 1994). In the unstable case the critical lines for the growing waves tend to lie on the poleward or equatorial flanks of the jet, and the mixing does not cross the jet maximum. The polar vortices of both hemispheres, therefore, tend to be quite well isolated during the winter season through much of their depth in the stratosphere despite the presence of large-amplitude propagating waves and local instabilities.

Acknowledgments. Steve Dahlberg provided much assistance with the power spectral calculations and other aspects of this project. This work was funded by NASA Grant NAGW-3446 to Texas A&M University.

REFERENCES

Bowman, K. P., 1993a: Barotropic simulation of large-scale mixing in the Antarctic polar vortex. *J. Atmos. Sci.*, **50,** 2901–2914.

——, 1993b: Large-scale isentropic mixing properties of the Antarctic polar vortex from analyzed winds. *J. Geophys. Res.*, **98,** 23 013–23 027.

——, 1995: Diffusive transport by breaking waves. *J. Atmos. Sci.*, **52,** 2416–2427.

——, and N. J. Mangus, 1993: Observations of deformation and mixing of the total ozone field in the Antarctic polar vortex. *J. Atmos. Sci.*, **50,** 2915–2921.

——, and P. Chen, 1994: Mixing by barotropic instability in a nonlinear model. *J. Atmos. Sci.*, **51,** 3692–3705.

Chen, P., 1994: The permeability of the Antarctic vortex edge. *J. Geophys. Res.*, **99,** 20 563–20 571.

——, J. R. Holton, A. O'Neill, and R. Swinbank, 1994: Quasi-horizontal transport and mixing in the Antarctic stratosphere. *J. Geophys. Res.*, **99,** 16 851–16 866.

Dahlberg, S. P., and K. P. Bowman, 1994: Climatology of large-scale isentropic mixing in the Arctic winter stratosphere from analyzed winds. *J. Geophys. Res.*, **99,** 20 585–20 599.

——, and ——, 1995: Isentropic mixing in the Arctic stratosphere during the 1992–1993 and 1993–1994 winters. *Geophys. Res. Lett.*, **22,** 1237–1240.

Hartmann, D. L., L. E. Heidt, M. Loewenstein, J. R. Podolske, J. Vedder, W. L. Starr, and S. E. Strahan, 1989: Transport into the south polar vortex in early spring. *J. Geophys. Res.*, **94,** 16 779–16 795.

Ishioka, K., and S. Yoden, 1994: Nonlinear evolution of a barotropically unstable circumpolar vortex. *J. Meteor. Soc. Japan,* **72,** 63–80.

Juckes, M., and M. E. McIntyre, 1987: A high resolution, one-layer model of breaking planetary waves in the stratosphere. *Nature,* **328,** 590–596.

Leovy, C. B., C.-R. Sun, M. H. Hitchman, E. E. Remsberg, J. M. Russell, L. L. Gordley, J. C. Gille, and L. V. Lyjak, 1985: Transport of ozone in the middle stratosphere: Evidence for planetary wave breaking. *J. Atmos. Sci.*, **42,** 230–244.

McIntyre, M. E., 1989: On the Antarctic ozone hole. *J. Atmos. Terr. Phys.*, **51,** 29–43.

——, and T. N. Palmer, 1983: Breaking planetary waves in the stratosphere. *Nature,* **305,** 593–600.

Nakamura, M., and R. A. Plumb, 1994: The effects of flow asymmetry on the direction of Rossby wave breaking. *J. Atmos. Sci.*, **51,** 2031–2045.

Pierce, R. B., and T. D. A. Fairlie, 1993: Chaotic advection in the stratosphere: Implications for the dispersal of chemically perturbed air from the polar vortex. *J. Geophys. Res.*, **98,** 18 589–18 595.

——, ——, W. L. Grose, R. Swinbank, and A. O'Neill, 1994a: Mixing processes within the polar night jet. *J. Atmos. Sci.*, **51,** 2957–2972.

——, W. L. Grose, J. M. Russell III, A. F. Tuck, R. Swinbank, and A. O'Neill, 1994b: Spring dehydration in the Antarctic stratospheric vortex observed by HALOE. *J. Atmos. Sci.*, **51,** 2931–2941.

Plumb, R. A., D. W. Waugh, R. J. Atkinson, P. A. Newman, L. R. Lait, M. R. Schoeberl, E. V. Browell, A. J. Simmons, and M. Loewenstein, 1994: Intrusions into the lower stratospheric Arctic vortex during the winter of 1991–1992. *J. Geophys. Res.*, **99,** 1089–1105.

Randel, W. J., 1990: A comparison of the dynamic life cycles of tropospheric medium-scale waves and stratospheric planetary-scale waves. *Dynamics, Transport and Photochemistry in the Middle Atmosphere of the Southern Hemisphere,* A. O'Neill, Ed., Kluwer, 91–109.

——, 1992: Global Atmospheric Circulation Statistics, 1000–1 mb. NCAR Tech. Note 366+STR, National Center for Atmospheric Research, Boulder, CO, 256 pp.

——, and I. M. Held, 1991: Phase speed spectra of transient eddy fluxes and critical layer absorption. *J. Atmos. Sci.*, **48,** 688–697.

——, and L. R. Lait, 1991: Dynamics of the 4-day wave in the Southern Hemisphere polar stratosphere. *J. Atmos. Sci.*, **48,** 2496–2508.

Salby, M. L., 1992: The influence of planetary-wave transience on horizontal air motions in the stratosphere. *J. Atmos. Sci.*, **49,** 405–421.

Schoeberl, M. R., and Coauthors, 1989: Reconstruction of the constituent distribution and trends in the Antarctic polar vortex from ER-2 flight observations. *J. Geophys. Res.*, **94,** 16 815–16 845.

——, L. R. Lait, P. A. Newman, and J. E. Rosenfield, 1992: The structure of the polar vortex. *J. Geophys. Res.*, **97,** 7859–7882.

Trenberth, K. E., and J. G. Olson, 1987: Evaluation of NMC global analyses: 1979–1987. NCAR Tech. Note NCAR/TN-229/+STR, National Center for Atmospheric Research, Boulder, CO, 82 pp.

Waugh, D. W., and Coauthors, 1994: Transport out of the lower stratospheric Arctic vortex by Rossby wave breaking. *J. Geophys. Res.*, **99,** 1071–1088.